Int j simul model 22 (2023) 2, 267-278
Original scientific paper

MODELLING ANALYSIS OF COUPLING DEFORMATION BETWEEN STRIP STEEL AND ROLLER SYSTEM

Cui, X. Y.[*]; Li, Z. Z.[*]; Yin, B. L.[**]; Wang, W. Q.[*]; Liu, Y. X.[***] & Bai, Z. H.[*,****,#]

[*] National Cold Rolling Strip Equipment and Process Engineering Technology Research Center of Yanshan University, Qinhuangdao 066004, China

[**] Tangshan Iron and Steel Group Co., Ltd., Tangshan 063000, China

[***] Engineering Research Center of Advanced Metal Composites Forming Technology and Equipment, Ministry of Education, Taiyuan University of Technology, Taiyuan 030024, China

[****] State Key Laboratory of Metastable Materials Science and Technology, Yanshan University, Qinhuangdao 066004, China

E-Mail: bai_zhenhua@aliyun.com ([#] Corresponding author)

Abstract
To reveal the characteristics of strip shape and roll change during the rolling process of six-high cold rolling mill (SHCRM), a three-dimensional finite element model of SHCRM was established by computer-aided design. The coupling deformation under various working conditions such as friction coefficient and bending roller force was analysed. Results show that the width of the plate, the amount of pressure, the friction coefficient, the rolling force, and the bending force are the key affecting factors of the deformation of the roller system, the shape of the load roll seam and the contact stress and strain. The deformation of the roll system, the shape change of the load roller seam and the stress and strain of the contact region are revealed. The obtained conclusions provide a reference for the development of rolling model of high cold rolling mill.
(Received in February 2023, accepted in May 2023. This paper was with the authors 1 months for 1 revision.)

Key Words: Six-High Cold Rolling Mill, Bending Roller, Roll Shifting, Loaded Roller Gap, Flatness

1. INTRODUCTION

The rapid development of industries such as aerospace, automotive, and electronics has increased the requirements of users for cold-rolled steel sheets and strips. The shape of cold-rolled steel sheets and strips has become one of the important indicators to measure the quality of finished steel strips [1, 2]. The quality of the strip shape directly affects the yield of the finished strip steel and the smooth processing of subsequent products, which is also the key to quality control of cold-rolled strip steel products [3, 4].

The strip is produced under the action of a deformed elastic body, that is, the roller, and the elastic deformation of the roller directly affects the cross-sectional shape of the final product. Therefore, the elastic deformation of the roller system plays an important role in the overall shape of cold strip mills. In general, if the elastic recovery deformation of the rolled strip is ignored, then the cross-sectional shape of the rolled strip is the load-bearing roll gap shape. Some disturbance factors such as the influence of rolling pressure changes on plate shape, as well as some plate shape control methods such as hydraulic bending rolls, are achieved through roll deformation. A harmful contact zone is usually formed outside the plate width due to the full length contact between the roller systems of the six-high cold rolling mill (SHCRM) along the roll body. This formation reduces the lateral stiffness of the rolling mill and affects the shape and crown of the rolled product. At the same time, the ability of the bending rolls to adjust the shape is greatly reduced. Therefore, optimizing roll shape selection and formulating roll lateral displacement plans are vital to study the effects of rolling and bending forces on the shape of loaded roll gaps during the rolling process, the influence and

elimination of the range of harmful contact areas between intermediate rollers due to the lateral displacement of intermediate rollers, and the effect on the shape of loaded roll gaps.

This study aims to analyse the effects of parameters such as strip width, bending force, reduction, and roll displacement on the force on the strip and roll during the rolling process of SHCRM. The influence on the loaded roll gap is also examined. The finite element simulation method is used to study the strip rolling process and obtain the stress distribution in the deformation zone and the loaded roll gap distribution during the rolling process.

2. STATE OF THE ART

At present, the related studies on the cold rolling process can be summarized into two main aspects. One is the distribution of stress and strain in the deformation zone of the strip steel during rolling, and the other is the distribution of loaded roll gaps during the rolling process. The two aspects can provide a reference for the study of the influence of deformation of the SHCRM on the deformation of the workpiece and roller system [5, 6].

Some scholars have studied the stress and strain of strip steel during the rolling process of an SHCRM. For examples, Eid and Sadawy investigated the effective strain in the role of AISI 304 austenitic stainless steel in cold rolling deformation by using optical, field emission scanning electron microscopy, X-ray diffraction, microhardness, and tensile stress–strain testing methods [7]. Chen et al. established a new deformation resistance model for strip steel using segmented functions. The mechanical performance could be described at any position by this model [8]. Baranov proposed a new solution to the Karman equation, which considerably improved the calculation accuracy of contact stress and rolling force by considering the reduction area of contact stress and the shape of the strip hardening curve [9]. Antonov et al. mathematically described the stress and strain in the rolls of a four-high rolling mill and studied the effects of axial displacement and hydraulic bending of the work rollers on the stress–strain state of the work rollers in cold rolling [10]. Kaliyev et al. developed a three-dimensional model of the rolling process and they obtained the equivalent stress and temperature field distribution of the strip steel under a single stand [11]. Milenin et al. established an elastic–plastic model for the laminar cooling process of hot-rolled strip steel and a deformation model for the inside of the strip steel coil [12]. Shatalov et al. studied the effect of lubricants on the stress and deformation indicators of the copper strip [13].

Other scholars have explored the loaded roll gap during the rolling process. Yan et al. conducted the dynamic simulation of the rolling process and obtained distribution curves of important rolling parameters such as equivalent stress, control efficiency coefficient, transverse rolling pressure, side thickness, and work roller deflection [14]. Kapil et al. developed the control equation for the motion of the work roller of a four-high rolling mill using finite element method and studied the vibration under different process parameters [15]. Stockert et al. analysed the applicability of combining highly dynamic piezoelectric actuators with electromechanical spindles, as well as high-frequency precision measurement of thickness before roll gap [16]. John et al. developed a rolling force model to calculate the rolling force of each stand, and the calculated rolling force was combined with the roll wear model to better predict the strip shape [17]. Fukushima et al. proposed a new method for high-precision online shape prediction based on matrix models by considering rolling force and tension through experiments and finite element analysis [18]. Li et al. suggested a shape preset strategy to allocate the convexity of the finishing mill according to the size of the shape control domain of each frame [19].

Based on the deformation of strip and roll during the cold rolling process, this study divided the finite element mesh according to the actual assembly situation and structure of the roll, simplified the calculation process, and completed the analysis of the half rolling finite

element model of typical specification products. The force influencing on strip and roll during the rolling process and the loaded roll gap influencing on the roll were obtained.

3. METHODOLOGY

3.1 Model parameter settings

The 1/2 rolling finite element model was established to simplify the rolling process without changing the environment, which made simulating the rolling process more convenient.

During the three-dimensional rolling process, the changes in the roller system were represented by the bending deformation of the roll axis. To represent the deformation of the roller system throughout the entire length of the roll body, a 1/2 two-dimensional model was built [20-22]. Based on the process parameters of the 1450 cold rolling mill, the finite element model, the geometric parameters, and performance of the rolled piece were determined, as shown in Table I.

Table I: Main parameters of 1450 SHCRM and rolled parts.

Support roller diameter (mm)	**Intermediate roller diameter** (mm)	**Work roller diameter** (mm)	**Transverse displacement of intermediate roller** (mm)	**Elastic modulus of roller** (GPa)	**Elastic modulus of rolled piece** (GPa)
1250	490	420	−60 to 60	210	208
Support roller body length (mm)	**Work roller barrel length** (mm)	**Intermediate roller body length** (mm)		**Poisson's ratio of roller**	**Poisson's ratio of rolled parts**
1500	1450	1520		0.30	0.30

3.2 Geometric modelling and mesh generation

First, a two-dimensional model was built on the basis of the two-dimensional modelling method. During this process, the elements in the contact area and the upcoming contact area were encrypted and subdivided. Simple unit dimensions were built in the noncontact area. Then, the unit surface was stretched and expanded in three-dimensional to form a rolling roller. Next, the three-dimensional model of the shoulder was stretched and extended on the end face of the rolling roller. Finally, a rigid plane was established as the power device for rotating the roller.

When dividing the grid, only the accessible areas needed to be encrypted and divided to reduce the number of grid units. Meanwhile, the remaining grid units only needed to meet the calculation requirements. When dividing the work roller into grids, the actual assembly situation and the length of the rolled sheet were considered. The length of the encrypted arc was also made equal to the length of the rolled sheet. Finally, the rolling model shown in Fig. 1 was obtained.

The rolling model was first simplified prior to studying the deformation of the rolling roller system. Considering the symmetry of the rolling roller system and deformation, the finite element 1/2 model was considered the analysis object, and the specific transverse direction was regarded as 1/2 with the centre of the plate width as the symmetry plane, as shown in Fig. 2.

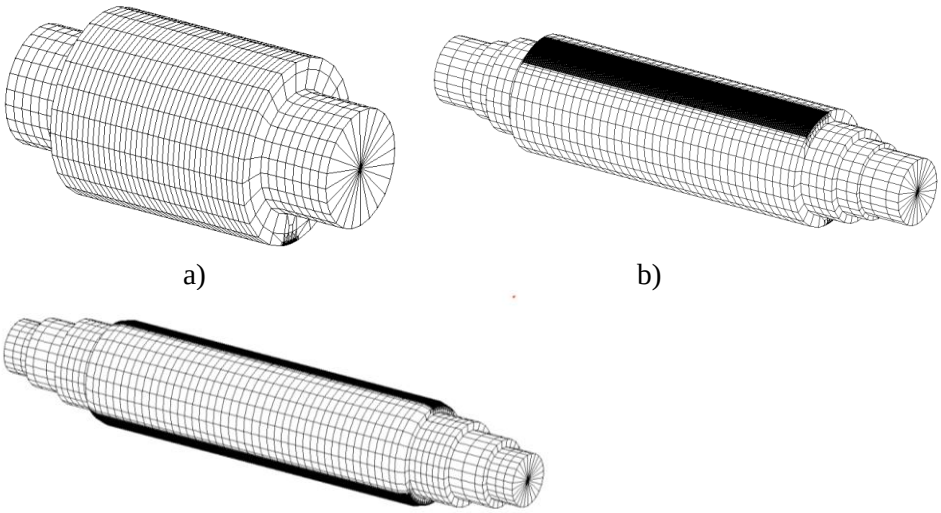

Figure 1: Roller grid of the model; a) Support roller mesh; b) Intermediate roller mesh; c) Work roller grid.

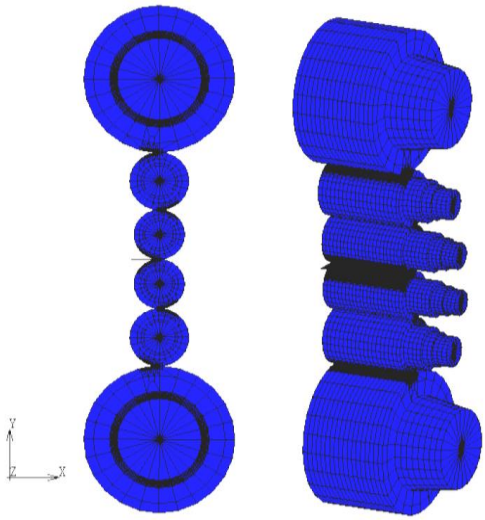

Figure 2: Rolling model of 1450 six roller system.

3.3 Boundary conditions

After the model was established, the pre-treatment operation of the rolling mill began. The support, intermediate, and work rollers were all treated according to the elastic body. In this working condition, the support roller was a press down driving roller, and the support roller moved downward to drive the overall roller system to press down, which achieved the plate press down working condition. The work roller was a rotating driving roller, and the rotation of the work roller drove the intermediate roller through friction to drive the support roller to rotate. This condition required the use of the large displacement option. By directly contacting the rigid body and the roller according to the bonding setting, the rotation of the rigid body was used to drive the rotation of the elastic roller.

At the same time, the central end face of the roller body was symmetrically treated, and the displacement in the *x*-direction of all rollers in the roller system was fixed to prevent the left and right deviation of the rollers from affecting the simulation analysis. Applying a rotation centre to all the rolls in the roller system provided constraints that the rolls could rotate. Using displacement constraints for reduction processing, the displacement constraints

in the *y*-direction were applied to the upper and lower support rollers. The sum of displacement amounts was the reduction amount of the rolling mill. The bending force was applied to the upper and lower work rollers and the upper and lower intermediate rollers. The bending force of the intermediate and work rollers differed. Front and rear tensions were applied to the plate to make it straight during the rolling process, and then, the function of a coiler could be achieved. Rotational speed was applied to the centre of the upper and lower work rollers as the driving force, which caused the entire roller system to rotate accordingly. Ultimately, the entire rolling simulation process was completed. The division of contact unit between roll and workpiece is shown in Fig. 3, the grid of 1/2 rolling calculation model workpiece is shown in Fig. 4, and the distribution of initial strength of workpiece is shown in Fig. 5.

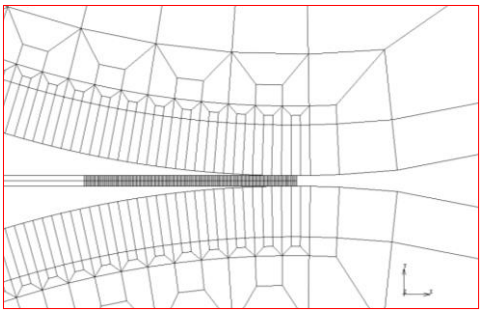

Figure 3: Division of contact units between rollers and workpieces.

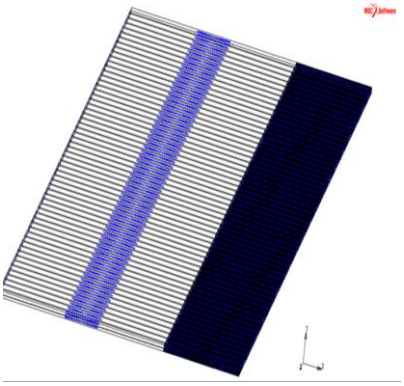

Figure 4: Rolled piece grid of 1/2 model.

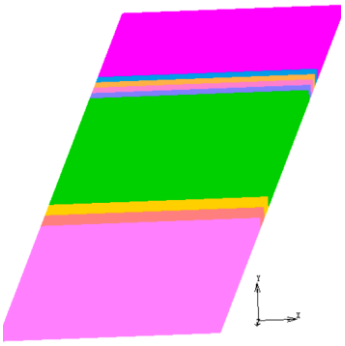

Figure 5: Initial strength distribution of model.

The specific rolling constraints were as follows. For the displacement constraint, the nodes on the lower end face of the rolled piece were fixed. The nodes on the fixed bottom surface also served as the upper and lower symmetry planes due to the symmetry of the rollers. The displacement in the *x*-direction of the work roller was set to 0, which limited the movement of the work roller in the *x*-direction. The rotation of the work roller around the *z*-axis was given a certain speed as the power device. The displacement in the *x*-direction of the intermediate roller was set to 0, which limited the movement of the intermediate roller in the *x*-direction. The rotation of the intermediate roller around the *z*-axis was not given a rotational speed, but it only served as a support axis for rotation. The displacement of the support roller in the *x*-direction was set to 0, which limited the movement of the support roller in the *x*-direction. The displacement of the support roller in the *y*-direction was set to nonlinear movement, which represented the pressing device. The rotation of the support roller around the *z*-axis was not given a rotational speed and only served as the rotational support axis. The nodes of the rear end faces of the rolled piece and the roller were fixed. The nodes of the fixed end face were used as the left and right symmetry planes due to the symmetry of the rollers. With regard to the concentrated force, the supported forces of the work and intermediate

rollers were regarded. For the unit surface distribution force, pre and post rolling tensions were considered.

4. RESULTS AND DISCUSSION

4.1 Analysis of force simulation for strip steel and rolling rolls

Effect analysis of plate width on contact strain and stress between rollers and plates: As shown in Fig. 6, the plastic deformation at the edge of the rolled piece is relatively large when the plate width is 1000 mm. The plastic deformation decreases from the edge to the inside under the same plate width. When the plate width is increased to 1100 mm, the degree of plastic deformation in the width direction is equal. However, the plastic deformation at the centre is relatively large when the plate width is increased to 1300 mm. The plastic deformation also gradually decreases from the middle to the edge under this plate width. Therefore, increasing the plate width appropriately can effectively improve the shape and quality of the rolled piece.

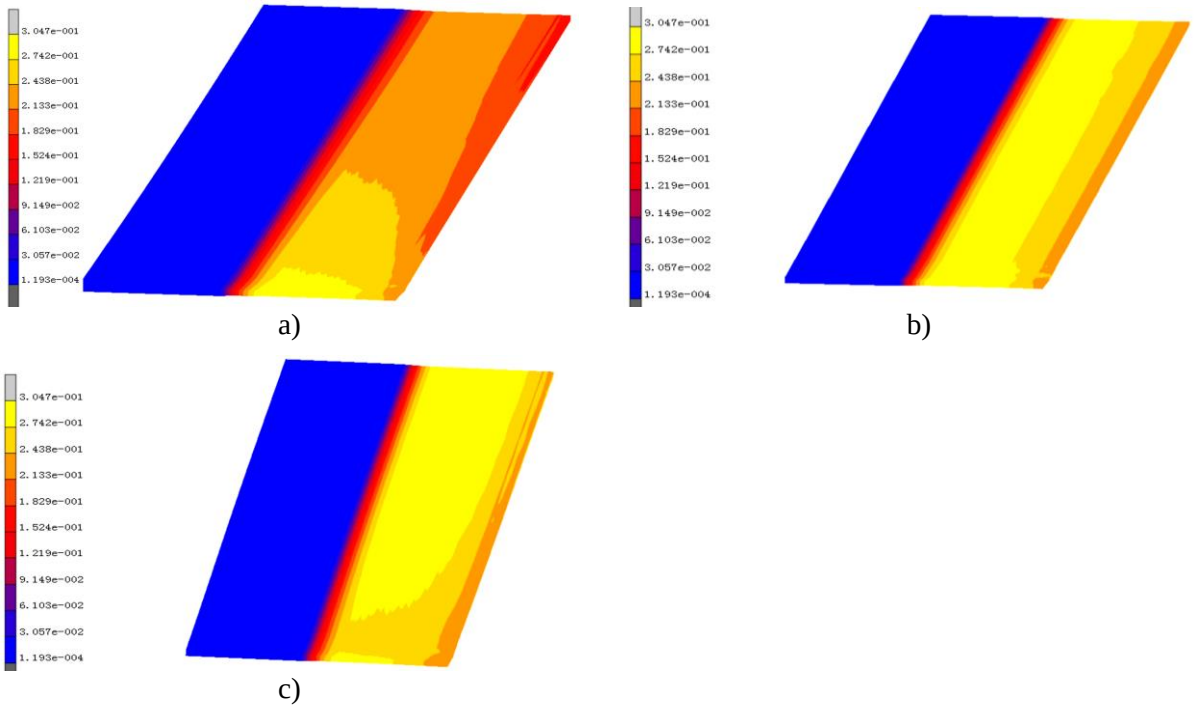

Figure 6: Plastic deformation under different plate widths; a) Plate width of 1000 mm; b) Plate width of 1100 mm; c) Plate width of 1300 mm.

The Mises equivalent stress on the half edge of the rolled piece is shown in Fig. 7. The maximum contact stress corresponding to the three plate widths is around 380 MPa, and the contact stress in the contact area between the roller and the strip steel is between 320 and 380 MPa.

Analysis of contact stress and strain between roll and plate under bending force: The Mises equivalent stress between the sheet metal and the work roller varies with the bending roll force is shown in Fig. 8. However, the maximum calculated stress values in the figure are around 380 MPa, and the contact stress in the contact area between the sheet metal and the roll is also between 300 and 370 MPa.

As shown in Fig. 9, the plastic deformation at the edge of the rolled piece is relatively large when the bending force is 400 kN. The plastic deformation decreases from the edge to the inside under the same bending force. When the bending force is increased to 600 kN, the

plastic strain in the width direction of the rolled piece is equal. However, a small part of the edge and most of the centre have larger plastic deformation when the bending force is increased to 800 kN. The plastic strain also gradually decreases from both ends to the middle under this bending force. Therefore, increasing the bending force appropriately can effectively improve the shape and quality of the sheet metal.

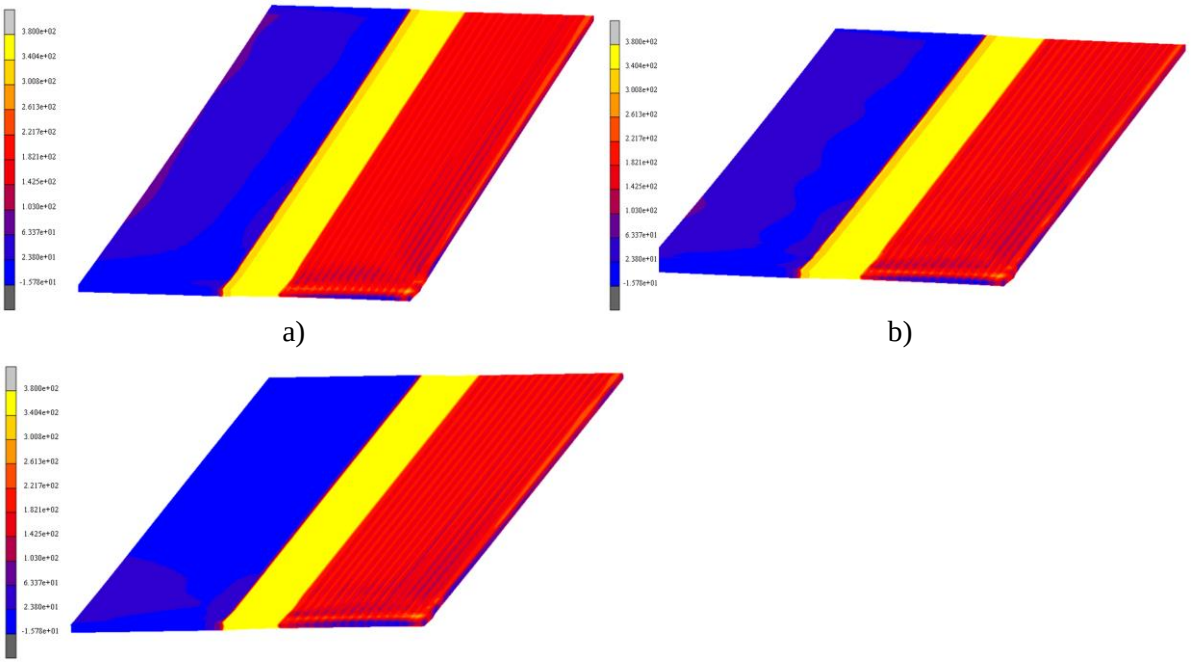

a) b)

c)

Figure 7: Equivalent stress under different plate widths (MPa); a) Plate width of 1000 mm; b) Plate width of 1100 mm; c) Plate width of 1300 mm.

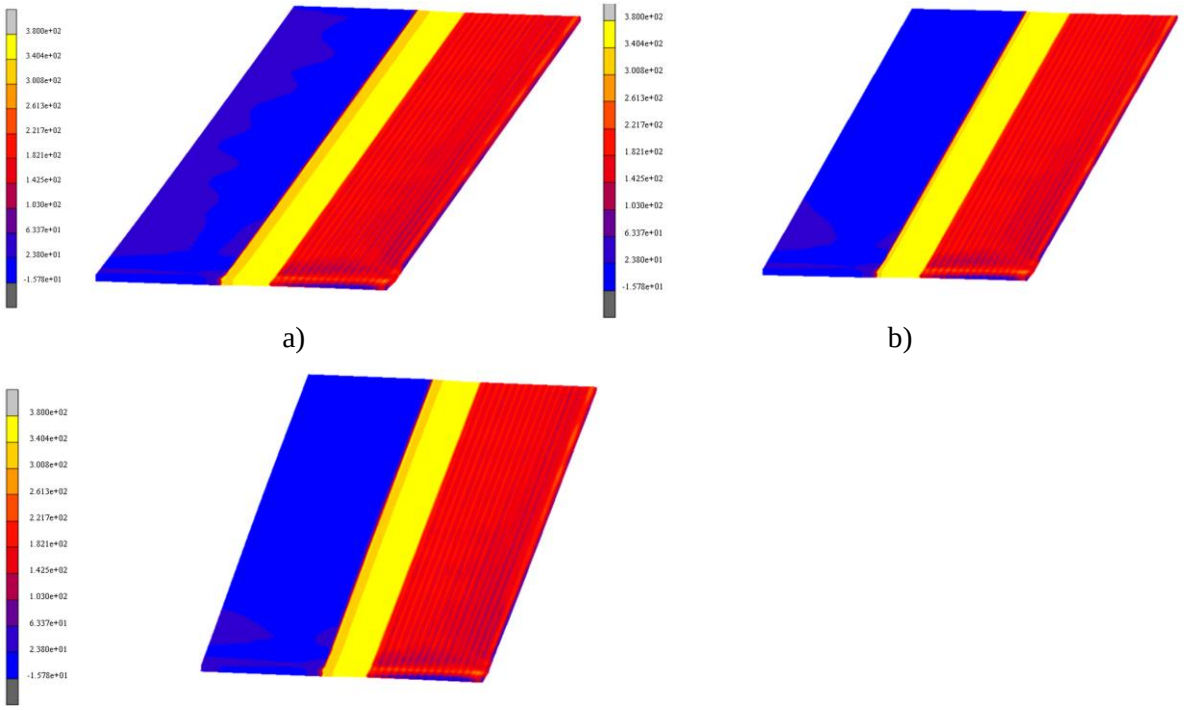

a) b)

c)

Figure 8: Equivalent stress under different bending roller forces (MPa); a) Bending roller force of 400 kN; b) Bending roller force of 600 kN; c) Bending roller force of 800 kN.

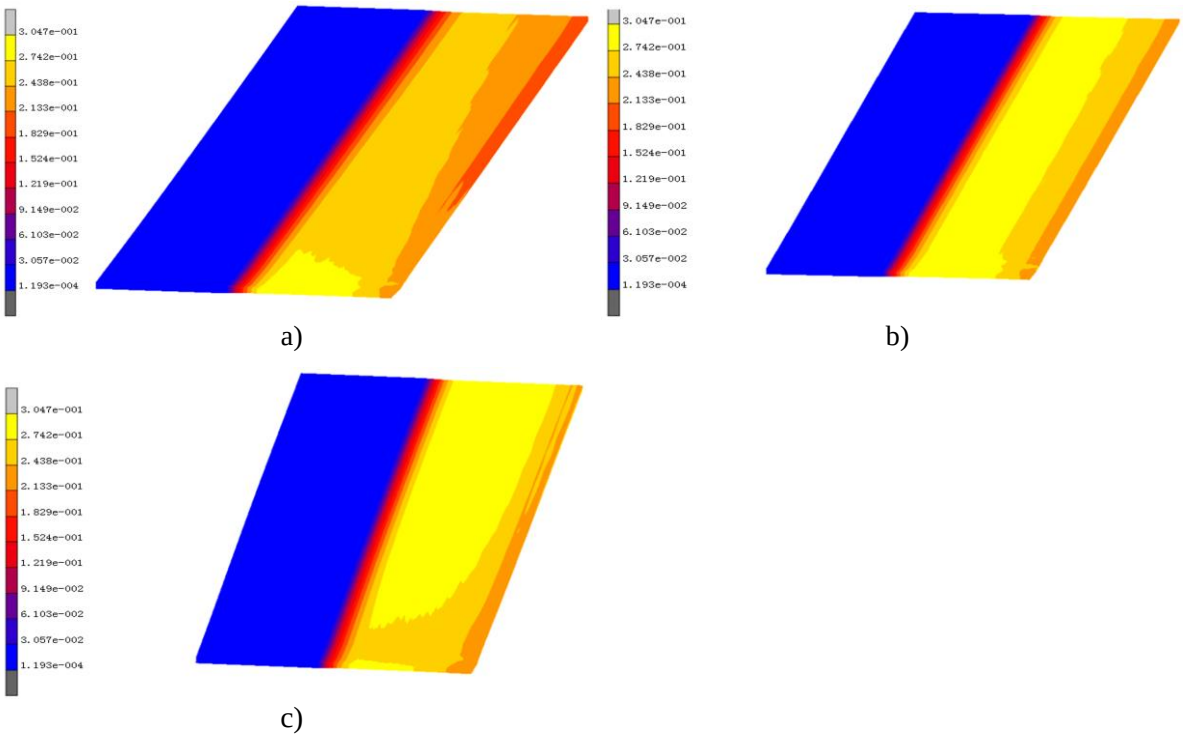

Figure 9: Equivalent stress under different bending roller forces (MPa); a) Bending roller force of 400 kN; b) Bending roller force of 600 kN; c) Bending roller force of 800 kN.

4.2 Analysis of loaded roll gaps in rolling mills

Owing to the close contact between the upper and lower work rollers and the sheet metal after stable rolling, the shape of the roll gap in the contact area is consistent with the shape of the exit section of the rolled piece. The study of the roll gap shape of the roll refers to the analysis of the exit section shape of the sheet metal, and the influence of lateral displacement and bending force on the roll gap shape is calculated. The basic parameters of the equipment and strip steel for simulating the rolling process are shown in Table II.

Table II: Parameter settings for strip steel and rolling mill.

Front tension (kN)	**Post tension** (kN)	**Bending roller force** (kN)	**Pressing amount** (mm)	**Friction coefficient**
130	80	400	210	0.05
Yield strength (MPa)	**Strip steel thickness** (mm)	**Strip width** (mm)	**Young's modulus** (GPa)	**Poisson's ratio**
620	2.2	1182	210	0.30

Influence of roll displacement on loaded roll gap: The amount of roll movement will affect the shape of the roll gap and thus the cross-sectional shape of the rolled piece. In analysing the shape of the roll gap between the upper and lower work rollers by changing the amount of roll movement of the intermediate rollers, the amount of roll movement of the upper and lower intermediate rollers is equal and opposite in direction. Except for changing the amount of roll movement, all other values are fixed. Thus, more rigorous and accurate results can be obtained. Each roll shifting amount is set as one working condition, which results in a total of four working conditions.

The shape of the roll gap is represented by the sum of node displacement and original position. The nodes in the contact area of the work roller are extracted using Marc software.

The *y*-axis is the sum of the selected node and original displacements, and the *x*-axis is the axial distance of the work roller.

As shown in Fig. 10, the entrance shape of the roll gap is rectangular before the rolled piece enters. After stabilizing through six rolls, the middle of the roll gap gradually decreases toward the edge of the roll. The reason is that the reaction force of the rolling force is generated after the plate enters the roll gap entrance. The work roller also undergoes flattening and elastic bending deformations.

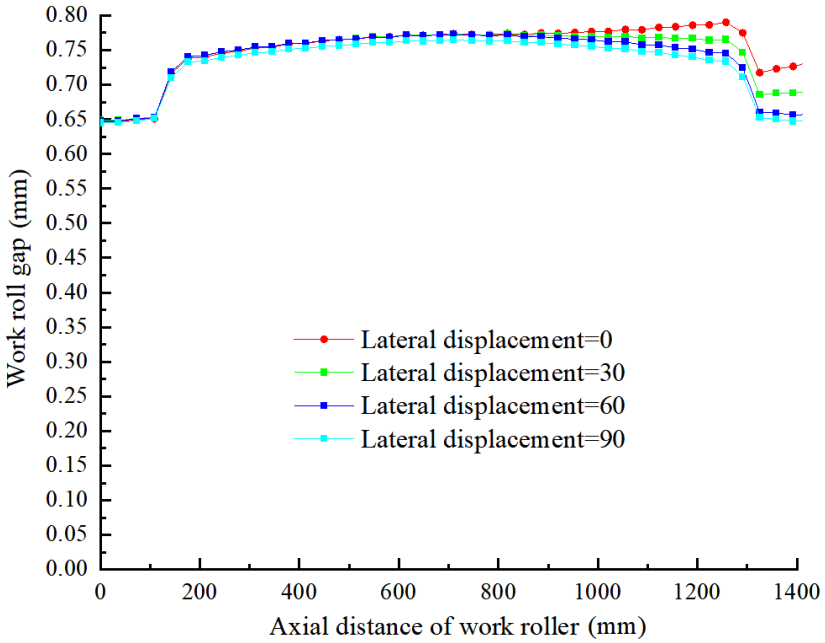

Figure 10: Curve of loaded roll gap under different roll shifting values.

The width of the rolled piece is smaller than the length of the work roller body. Thus, no contact is applied between the roll gaps beyond the width of the plate. Therefore, edge thinning occurs in the contact boundary area of the plate. Accordingly, this contact area is also a harmful contact area, and the roll gap distance outside the harmful contact area is the shortest. For the loaded roll gap curves of six rolls rolling with four different roll shifting amounts, the roll gaps show concave shapes when the roll shifting amounts are 0 and 30 mm. The shape of the roll gap is straight when the roll displacement is 60 mm. The shape of the roll gap gradually shows a downward convex shape when the roll displacement is 90 mm. However, only the outer end of the roll gap centre undergoes deformation, that is, the deformed part of the roll gap gradually rises from a downward direction as the amount of roll movement increases. A critical value of roll movement that makes the roll gap straight exists, but the half that has not undergone deformation still shows a half concave shape.

The shape of the roll gap and the cross-sectional shape of the sheet metal are consistent. As a result, the roll gap changes from concave deformation to straight and then becomes convex as the amount of roll shifting increases. Therefore, for sheet metal rolling parts, the cross-sectional shape of the sheet metal changes from convex deformation to straight and then to concave as the amount of roll shifting increases. In actual rolling processes, increasing the appropriate amount of roll shifting can improve the central convexity or edge flatness of the rolled product.

Influence of bending force on loaded roll gap: The bending force not only affects the bending deformation of the roller system but also may influence the shape of the roll gap. During the rolling process, only the work roller bending force is changed. Three types of

bending forces are set, and the other values are set to fixed values. The other parameters are shown in Table II.

The roll gap curves under the action of three different bending forces are shown in Fig. 11. The bending force continues to increase, and the shape of the roll gap gradually changes from concave to straight. The roll gap curve continues to deform and eventually becomes convex as the bending force continues to increase. Moreover, the height difference between the roll gap in the contact area and the noncontact area continues to decrease as the bending force increases. The height of the roll gap in the contact area also changes inconsiderably. The shape of the roll gap changes. The height of the roller gap in the noncontact area at both ends gradually increases, and the shape of the roller gap gradually becomes warped from the middle to both ends.

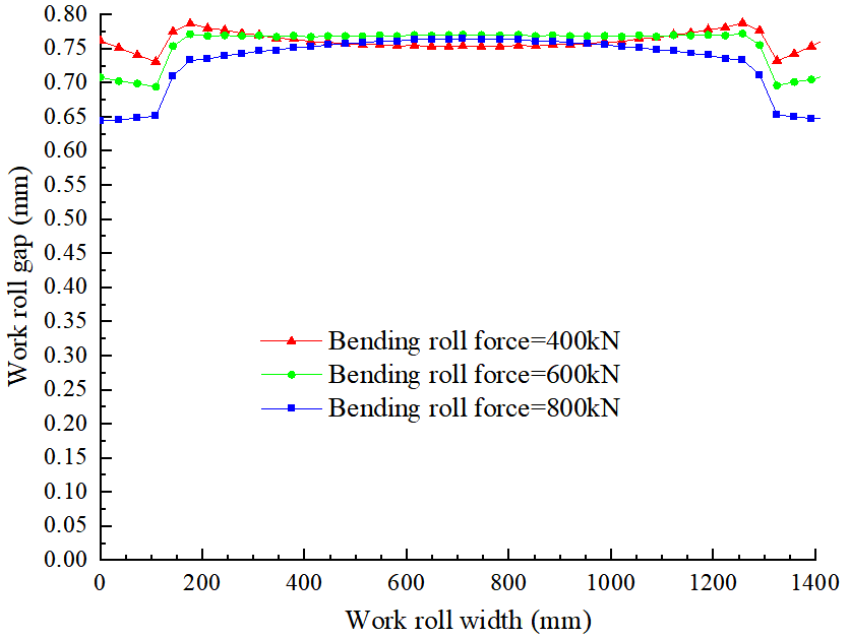

Figure 11: Curve of loaded roll gap under different bending forces.

The issue of plate shape is exactly the opposite of the change in roll gap. However, for plate shape, only the contact area (including harmful contact areas) needs to be analysed. Therefore, the central shape of the plate gradually becomes straighter from convex as the bending roller force gradually increases. However, the shape of the plate changes from straight to concave with the further increase in bending roller force. Therefore, an appropriate size of bending force can be selected to ensure the flatness of the sheet shape.

When the roll displacement is 60 mm, the contact area of the roll gap shape is relatively straight, and the height of the roll gap changes considerably. The shape of the roller gap is flatter and the height of the roller gap is higher when the reduction is smaller. The roller gap shape is the most stable when the reduction is 0.8 mm. The friction coefficient considerably affects the height of the roll gap shape. Specifically, the elastic deformation between the rolls increases and the entire roll moves upward as the friction force rises. Therefore, the height of the roll gap shape increases as the friction coefficient rises. The bending force inconsiderably affects the height of the roll gap shape, but it remarkably influences the shape of the roll gap in the contact area. The plate shape is relatively straight and the quality of the rolled piece is better when the bending force is 600 kN. The simulation results are consistent with the actual on-site production conditions, and they can guide the adjustment of on-site production process parameters.

5. CONCLUSIONS

By establishing a 1/2 finite element model, the rolling process of an SHCRM was simulated, and the stress on the strip steel and rolls during the rolling process was studied. The influence of loaded roll gaps was also simulated. The main conclusions are as follows.

(1) For sheet metal rolling parts, the cross-sectional shape of the sheet metal changes from convex deformation to straight and then to concave as the amount of roll shifting increases. In actual rolling processes, increasing the appropriate amount of roll shifting can improve the central convexity or edge flatness of the rolled product.

(2) For the deformation of the central axis of the work roller, the reduction amount should be chosen as 0.8 mm, and the friction coefficient should also be chosen as 0.05. The plate width should not be too wide or long, such as 1182 mm, and the roll displacement amount should be chosen as 60 mm.

(3) The plate shape is relatively straight and the quality of the rolled piece is good when the bending force is 600 kN. The shape of the roller gap in the contact area is relatively straight when the plate width is 1300 mm. The length of the harmful contact area decreases and becomes straighter under this plate width.

This study provides a reference for the calculation and simulation of the distribution of loaded roll gaps in the SHCRM. However, the actual cold rolling process is complex and has many influencing factors. Therefore, multiple factors should be considered in combination with on-site production practice and the distribution of loaded roll gaps should be simulated in a more detailed and comprehensive manner to provide theoretical support for improving the quality of finished strip steel.

ACKNOWLEDGEMENT

This work was supported by Science and Technology Project of Hebei Education Department (CXY2023012), Special Project for Transformation of Major Scientific and Technological Achievements in Hebei Province (22281001Z), and the Basic Project of Higher Education Institutions of Liaoning Province (LJKZZ20220040), China.

REFERENCES

[1] Olaogun, O.; Edberg, J.; Lindgren, L.-E.; Oluwole, O. O.; Akinlabi, E. T. (2019). Heat transfer in cold rolling process of AA8015 alloy: a case study of 2-D FE simulation of coupled thermo-mechanical modeling, *The International Journal of Advanced Manufacturing Technology*, Vol. 100, No. 9-12, 2617-2627, doi:10.1007/s00170-018-2811-2

[2] Zhang, W. J.; Zhang, X. D.; Guo, Z. F.; Wang, J. H.; Bai, Z. H. (2023). Simulation analysis of temperature field of tinplate in the quenching, *International Journal of Simulation Modelling*, Vol. 22, No. 1, 88-99, doi:10.2507/IJSIMM22-1-634

[3] Imai, T.; Utsunomiya, H.; Matsumoto, R. (2017). Finite element analysis of plastic instability phenomenon in cold rolling of clad sheets, *Procedia Engineering*, Vol. 184, 306-312, doi:10.1016/j.proeng.2017.04.099

[4] Liu, G. F.; Cui, X. Y.; Li, Z. Z.; Wang, J. H.; Zhang, X. D.; Bai, Z. H. (2022). Shape change simulation analysis of wheel steel in a four-high hot rolling mill, *International Journal of Simulation Modelling*, Vol. 21, No. 4, 603-614, doi:10.2507/IJSIMM21-4-621

[5] Yoon, S. J.; Shin, T. J.; Lee, J. S.; Hwang, S. M. (2017). Three-dimensional finite element analysis of skin-pass rolling and new models for process control, *Journal of Manufacturing Science and Engineering*, Vol. 139, No. 9, Paper 091003, 10 pages, doi:10.1115/1.4036910

[6] Wang, G. D.; Wang, H. Y.; Jiang, L. (2022). Parameter optimization of aeroengine blade rolling forming process based on finite element simulation, *Forging & Stamping Technology*, Vol. 47, No. 3, 109-115, doi:10.13330/j.issn.1000-3940.2022.03.017

[7] Eid, E. A.; Sadawy, M. M. (2021). Role of effective strain during cold rolling deformation on mechanical characteristics of AISI 304 steel, *Metals and Materials International*, Vol. 27, No. 11, 4536-4549, doi:10.1007/s12540-020-00722-9
[8] Chen, L. Z.; Sun, W. Q.; He, A. R.; Liu, C. (2022). Study on quarter-wave generation mechanism in DP980 steel during cold rolling, *The International Journal of Advanced Manufacturing Technology*, Vol. 120, No. 1-2, 313-327, doi:10.1007/s00170-021-08395-3
[9] Baranov, G. L. (2022). Refined technique for calculating contact stresses during the strip cold rolling, *Steel in Translation*, Vol. 52, No. 9, 874-879, doi:10.3103/S0967091222090029
[10] Antonov, P. V.; Bolobanova, N. L.; Kozhevnikova, I. A. (2019). Roller stress and strain in a broad-strip cold-rolling mill, *Steel in Translation*, Vol. 49, No. 5, 339-344, doi:10.3103/S0967091219050024
[11] Kaliyev, Y. B.; Baizhumanov, K. D.; Tursymbekova, Z. Z.; Thumanov, M. A.; Smailova, G. A.; Azilkiyasheva, M. M.; Zhauyt, A. (2021). Study of stress-strain state billets when rolling in a continuous mill of hot-rolled thin stripes using MSC super forge, *Metalurgija*, Vol. 60, No. 1-2, 159-161
[12] Milenin, A.; Kuziak, R.; Lech-Grega, M.; Chochorowski, A.; Witek, S.; Pietrzyk, M. (2016). Numerical modeling and experimental identification of residual stresses in hot-rolled strips, *Archives of Civil and Mechanical Engineering*, Vol. 16, No. 1, 125-134, doi:10.1016/j.acme.2015.08.002
[13] Shatalov, R. L.; Chan, V. Q.; Pham, V. H. (2022). Effect of roll lubricants on the deformation and force indicators and the strip sizes during cold rolling of copper, *Russian Metallurgy (Metally)*, Vol. 2022, No. 13, 1809-1813, doi:10.1134/S0036029522130353
[14] Yan, Z.-W.; Wang, B.-S.; Bu, H.-N.; Li, H.; Hong, L.; Zhan, D.-H. (2022). Comprehensive analysis of metal deformation law based on numerical simulation of cold rolling process, *Archives of Metallurgy and Materials*, Vol. 67, No. 2, 623-635, doi:10.24425/amm.2022.137799
[15] Kapil, S.; Eberhard, P.; Dwivedy, S. K. (2016). Dynamic analysis of cold-rolling process using the finite-element method, *Journal of Manufacturing Science and Engineering*, Vol. 138, No. 4, Paper 041002, 10 pages, doi:10.1115/1.4031280
[16] Stockert, S.; Wehr, M.; Lohmar, J.; Hirt, G.; Abel, D. (2018). Improving the thickness accuracy of cold rolled narrow strip by piezoelectric roll gap control at high rolling speed, *CIRP Annals*, Vol. 67, No. 1, 313-316, doi:10.1016/j.cirp.2018.04.107
[17] John, S.; Sikdar, S.; Mukhopadhyay, A.; Pandit, A. (2006). Roll wear prediction model for finishing stands of hot strip mill, *Ironmaking & Steelmaking*, Vol. 33, No. 2, 169-175, doi:10.1179/174328106X80091
[18] Fukushima, S.; Washikita, Y.; Sasaki, T. (2014). Mixed scheduled rolling of high tensile strength and mild steel using a high-accuracy profile model in hot strip finishing mill, *Tetsu-to-Hagane*, Vol. 100, No. 12, 1499-1507, doi:10.2355/tetsutohagane.100.1499
[19] Li, H.-J.; Zhao, X.-L.; Xu, J.-Z.; Wang, G.-D.; Xiao, Y. (2009). Shape presetting strategy for hot strip mills, *Journal of Iron and Steel Research*, Vol. 2009, No. 10, 17-20, doi:10.13228/j.boyuan.issn1001-0963.2009.10.005
[20] Wang, S. R.; Xiao, H. G.; Zou, Z. S.; Cao, C.; Wang, Y. H.; Wang, Z. L. (2019). Mechanical performances of transverse rib bar during pull-out test, *International Journal of Applied Mechanics*, Vol. 11, No. 5, Paper 1950048, 15 pages, doi:10.1142/S1758825119500480
[21] Luo, T.; Wang, S. R.; Zhang, C. G.; Liu, X. L. (2017). Parameters deterioration rules of surrounding rock for deep tunnel excavation based on unloading effect, *DYNA*, Vol. 92, No. 6, 648-654, doi:10.6036/8554
[22] Wang, S.-R.; Liu, Z.-W.; Qu, X.-H.; Fang, J.-B. (2009). Large deformation mechanics mechanism and rigid-gap-flexible-layer supporting technology of soft rock tunnel, *China Journal of Highway and Transport*, Vol. 22, No. 6, 90-95